Atom Indonesia

Journal homepage: http://atomindonesia.brin.go.id

PHITS-Based Simulation of Dose Distributions and Secondary Particle Fluence from Light and Heavy Ions at Therapeutic Energies in a Water Phantom

C. G. M. Dalumpines*, G. F. I. Peñonal, H. P. Aringa, V. C. Convicto

Computational Medical and Radiation Physics Group, Department of Physics, Mindanao State University, Marawi City 9700, Lanao del Sur, Philippines

ARTICLE INFO

Article history:
Received 27 February 2025
Received in revised form 3 June 2025
Accepted 17 June 2025

Keywords:

Cancer
Heavy ions
Fluence
PDD
PHITS

ABSTRACT

Comprehensive dosimetric evaluation of light and heavy ions such as protons, alpha particles, carbon, and oxygen ions is essential for advancements in radiation therapy and space applications. This study employed the Particle and Heavy Ion Transport code System (PHITS) to simulate dose distributions and secondary particle fluence in a water phantom across a range of therapeutic ion energies. A 30 × 30 × 30 cm³ water phantom with 2.0×10^8 primary particles at a Source to Surface Distance (SSD) of 100 cm were irradiated using mono energetic axial source. This simulation study also evaluated particle fluence of secondary particles such as electrons, positrons, and neutrons. Results showed that positron fluence concentrates around the water phantom, dispersing more at higher energy, while neutron flux focuses along the source path. The PHITS generated Percent Depth Dose (PDD) curves illustrate varied dose deposition patterns for each ion at different energies. For the highest energy considered, the simulated Bragg peak positions deviated by not more than 4.55% from the experimental data, with simulation uncertainties kept below 0.1%, ensuring accurate dose analysis. Helium ions (alpha particles) exhibited favorable treatment characteristics such as lower entrance dose, minimal lateral scattering, and reduced fragmentation consistent with the experimental findings. Additionally, the spatial distributions of electrons, positrons, and neutrons show elevated concentrations near the water phantom, indicating potential benefits for enhancing treatment precision.

INTRODUCTION

With rising rates of morbidity and mortality, cancer is a significant worldwide public health concern. Hadron or particle therapy is one of its treatments, and the number of new particle therapy centers has increased dramatically in the last decade [1-3]. Particle beams such as protons and heavier ions possess distinct radiobiological effects compared to conventional photon based therapies, offering potential advantages in precision medicine, particularly in cancer treatment. The precise evaluation of their dose distributions and biological impacts is essential for optimizing therapeutic outcomes and minimizing damage to surrounding healthy tissues.

The Monte Carlo (MC) approach is recognized as the most accurate analytical methodology for creating tumor treatment plans in the field of medical radiation physics. Its application spans across various areas, and comprehensive reviews have been published. Several studies have demonstrated the superiority of the MC method in dose calculations, particularly in complex geometries, compared to conventional radiation therapy treatment planning systems [4-12]. One of the MC computational models is the Particle and Heavy Ions Transport code System (PHITS) and has proven to be a robust tool for simulating the transport and interaction of heavy ions with matter. Despite its accuracy, limited research has explored the dose distribution of heavy ions using the Particle and Heavy Ion Transport code System (PHITS) simulation platform. This study aims to

*Corresponding author.
E-mail address: clydegibb.dalumpines@msumain.edu.ph
DOI: https://doi.org/10.55981/aij.2025.1643

evaluate the depth dose distributions and secondary particle fluence of therapeutic ions proton (^{1}H), alpha (^{4}He), carbon (^{12}C), and oxygen (^{16}O) at various energies in a water phantom using PHITS. Secondary particles such as electrons, positrons, and neutrons were also analyzed to assess their contribution to the overall radiation field. Furthermore, the simulation results were compared with the experimental findings of Tessonnier et al. (2017) [13].

THEORY/CALCULATION

At the end of their range, heavier ions and protons deposit energy as they go through matter, resulting in a peak called the Bragg peak. A key concept in radiation physics and dosimetry is the rate of energy loss of a charged particle as it moves through a material, which is mostly caused by ionization and atom excitation. This rate, commonly referred to as stopping power S, designated as $-\frac{dE}{dx}$, is fundamental in understanding the interaction of particles with matter and is calculated using the Bethe Bloch formula given by Eq. (1).

$$-\frac{dE}{dx} = R\rho\frac{Z}{A}\frac{z^2}{\beta^2}\left[\ln\left(\frac{2m_e\gamma^2v^2T_{max}}{I^2}\right) - 2\beta^2 - \delta - 2\frac{C}{Z}\right] \quad (1)$$

The amount of energy that an ionizing particle imparts to the substance it passes through per unit distance is known as linear energy transfer (LET) and is correlated with the particle's mass [14,15].

METHODOLOGY

PHITS Monte Carlo simulation toolkit

The Particle and Heavy Ion Transport code System (PHITS) version 3.30, was used to perform MC simulations of a medical linac [16,17]. Using a variety of nuclear reaction models and data libraries, the PHITS code system is a general purpose MC Particle and Heavy Ion Transport code system that can estimate the transport of particles across any medium over a wide energy range. PHITS's accuracy and utility have been proven in a number of research fields, such as accelerator shielding studies, space radiation dosimetry, radiosurgery [10] and heavy ion radiotherapy [11,12,18].

Simulation set-up

A box shaped phantom of 30 × 30 × 30 cm^3 was employed in this investigation. Water was used as the phantom material, with the density of 1 g/cm^3. 2.0 × 10^8 primary particles from various radiation sources, including carbon (^{12}C), oxygen (^{16}O), alpha (^{4}He), and proton (^{1}H), were used to irradiate the phantom. Refer to Fig. 1 for the configuration of the simulation. Source to Surface Distance (SSD) was set at 100 cm. Four sets of initial energies per particle source were considered as these datasets share a comparable energy index from the energy tables, reflecting a similar range in water [17]. The initial energies for proton (^{1}H) were set at 54.19 MeV/u, 78.30 MeV/u, 101.90 MeV and 121.95 MeV. For alpha (^{4}He): 56.44 MeV, 79.78 MeV/u, 103.05 MeV/u and 122.93 MeV/u. For Carbon (^{12}C): 100.07 MeV/u, 145.47 MeV/u, 190.75 MeV/u and 229.76 MeV/u and for oxygen (^{16}O): 117.20 MeV/u, 171.03 MeV/u, 224.84 MeV/u and 271.59 MeV/u. The source of energy was an axial mono energetic source, and the size of the radial source was 0.10 cm.

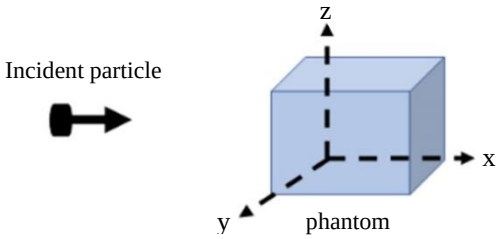

Fig. 1. Simulation set-up.

Percentage Depth Dose (PDD)

Dose data were calculated using the PHITS program tally depositiom and subsequentlyextracted for analysis.

Electron, positron, and neutron flux

Using tally tracks, the PHITS program was used to visualize and compute the flux of secondary particles, including electrons, positrons, and neutrons.

RESULTS AND DISCUSSION

Figure 2 displays the PDD curves for proton, alpha, carbon, and oxygen ions at different energies in water. The depth dose profile of each incident particle with four sets of initial energies are shown in Fig. 3. As shown, the PDD profiles for all the particle sources have tiny dosage at entrance, a dramatic rise in dose at a specific depth, and a quick decline in dose beyond the maximum dose deposition, or the Bragg peak, which was roughly where the incident beam range ends. By increasing the initial beam energy for each particle source, the Bragg peak position was moved to the deeper parts of the water phantom as shown in Table 1. The depth of maximum dose deposition, or Bragg

peak, rose with energy for all ion types investigated including proton (^{1}H), alpha (^{4}He), carbon (^{12}C), and oxygen (^{16}O). These peaks correlated to lower starting energy (~54 MeV for protons and ~118 MeV for oxygen) at a depth of about 2 cm. Bragg peaks moved deeper into the phantom with increasing energy, reaching roughly 4.5 cm, 7.5 cm, and 10.5 cm for increasingly higher energy levels. This pattern indicates that to reach penetration depths comparable to those of lighter ions, heavier ions need higher energy.

As shown, comparative analysis between the simulated Bragg peak positions and the experimental data presented by Tessonnier et al. [13] demonstrates that the percentage difference remains within 20 % for all ion species investigated. This deviation was within acceptable bounds for Monte Carlo simulations involving heavy ions, considering the complexity of nuclear interactions and medium heterogeneity. Additionally, the statistical uncertainty of the PHITS simulations was maintained below 0.1 %, ensuring high precision and confidence in the reported dose and fluence distributions. Helium ion, also known as the alpha particle, provides more conformal treatment because of its low entrance dosage, reduced lateral scattering, and decreased fragmentation, which aligns with the experimental findings [13].

Table.1. Comparison of the PHITS simulated and experimental range by Tessonnier et al., (2017) [13] at various incident energies for proton (^{1}H), alpha (^{4}He), carbon (^{12}C), and oxygen (^{16}O) ions in a water phantom.

Incident Energy of Light and Heavy Ions (MeV/u)				Range (cm)		
(^{1}H)	(^{4}He)	(^{12}C)	(^{16}O)	Exp. Data [13]	Monte Carlo Sim.	% Diff.
54.19	56.44	100.07	117.20	2.50	2.00	20.00
78.30	79.78	145.47	171.03	5.00	4.50	10.00
101.90	103.05	190.25	224.84	8.00	7.50	6.25
121.95	122.93	229.76	271.59	11.00	10.50	4.55

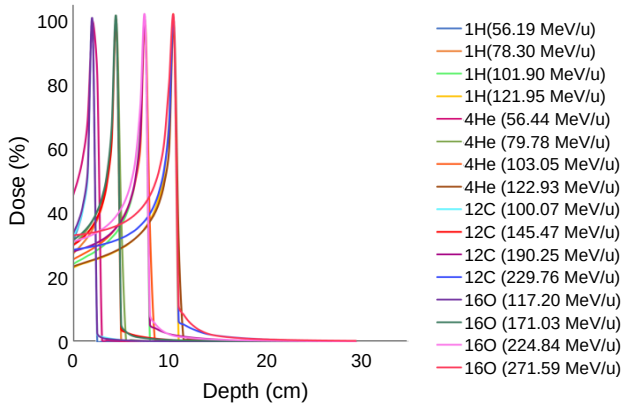

Fig. 2. Percent Depth Dose (PDD) profiles of proton (^{1}H), alpha (^{4}He), carbon (^{12}C), and oxygen (^{16}O) ions at various energy sources in water.

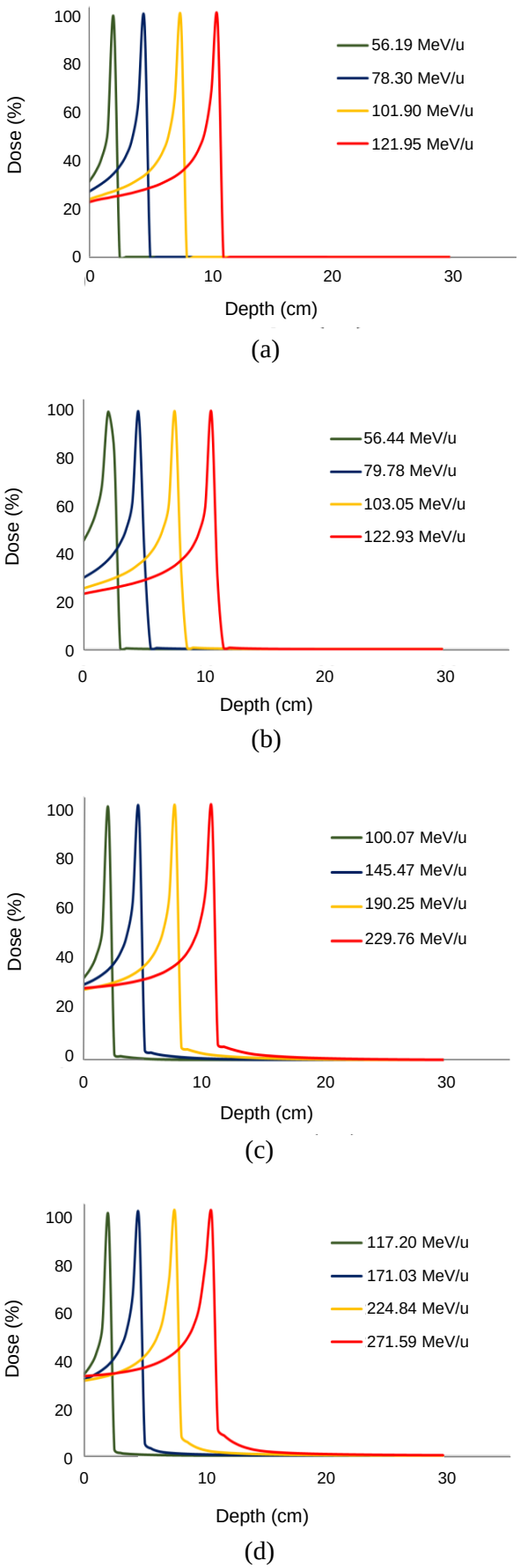

Fig. 3. PDD profiles for (a) proton(^{1}H), (b) alpha (^{4}He), (c) carbon (^{12}C), and (d) oxygen (^{16}O) ions at increasing energies in water.

For heavy ions like proton, alpha, carbon and oxygen yield secondary particles through nuclear interactions across the water phantom and experience straggling and nuclear fragmentation. This was evident in the presence of dose tails (see Figs. 2 and 3) which were caused by nuclear fragments via ionization processes. These secondary fragments in the tail were lighter compared to the incident ions. To have a longer range tails and lighter, are the primary drivers of the energy deposition that occur outside the incident primaries' range [19,20]. Interestingly, the Bragg peak and the lateral dose deposit both broaden with increasing incident energy, particularly for heavier ions. Clinically, these physical behaviors are significant because broader dose distributions and elevated secondary particle production especially neutrons can increase radiation exposure to nearby healthy tissues. Thus, selecting the appropriate ion type and optimizing treatment planning are critical for ensuring accurate dose delivery and minimizing unintended side effects in particle therapy.

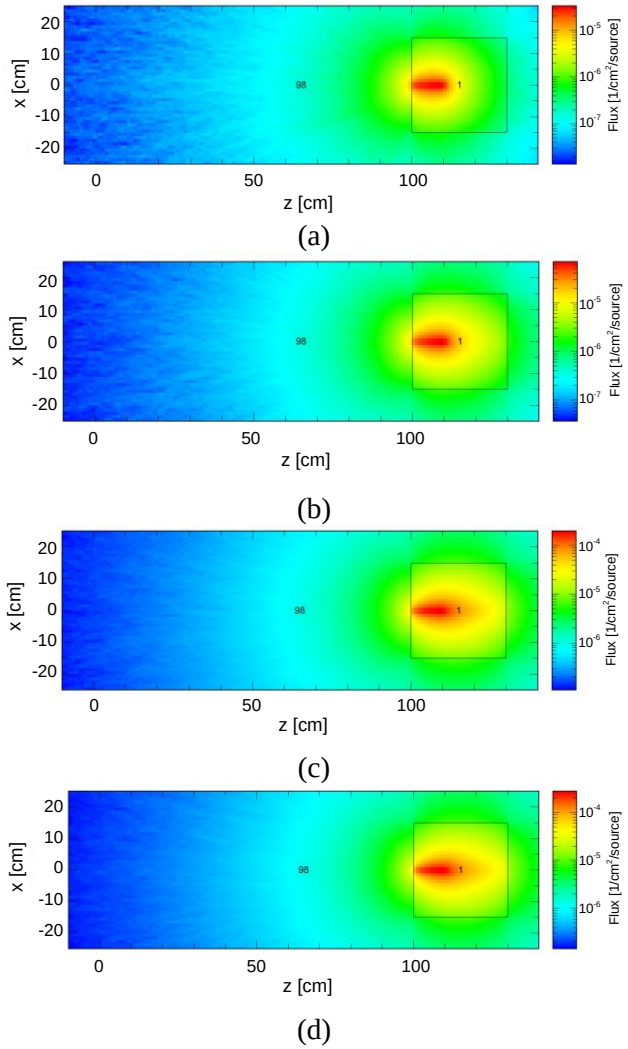

Fig. 4. Electron fluence distributions from (a) proton (^{1}H), (b) alpha (^{4}He), (c) carbon (^{12}C), and (d) oxygen (^{16}O) at energy of 121.95 MeV/u, 122.93 MeV/u, 229.76 MeV/u and 271.59 MeV/u, respectively.

Additionally, the spatial distributions of electron, neutron, and positron fluence of proton (^{1}H), alpha particles (^{4}He), carbon ions (^{12}C), and oxygen ions (^{16}O) at energies of 121.95 MeV/u, 122.93 MeV/u, 229.76 MeV/u and 271.59 MeV/u are shown in Figs. 4-6. Color gradients represent fluence intensity, with blue indicating the lowest and red the highest.

Electron fluence approximately 10^{-5} 1/cm^2/source for proton (^{1}H) and alpha (^{4}He), increasing to 10^{-4} 1/cm^2/source for carbon (^{12}C) and oxygen (^{16}O) ions. Neutron fluence showed a similar trend, ranging from 10^{-3} 1/cm^2/source for protons to 10^{-2} 1/cm^2/source for heavier ions. Positron fluence was the lowest among the three, increasing from 10^{-6} 1/cm^2/source for light ions to 10^{-5} 1/cm^2/source for carbon and oxygen.

These results indicate that the production of secondary particles increases with ion mass and energy. All three types electrons, neutrons, and positrons were primarily concentrated within the water phantom. Electron fluence was the lowest near the source across all ions. Neutron fluence formed a path from the source to the phantom, while positron intensity, although generally low, shifted from moderate near the source to lower intensities as n mass increases.

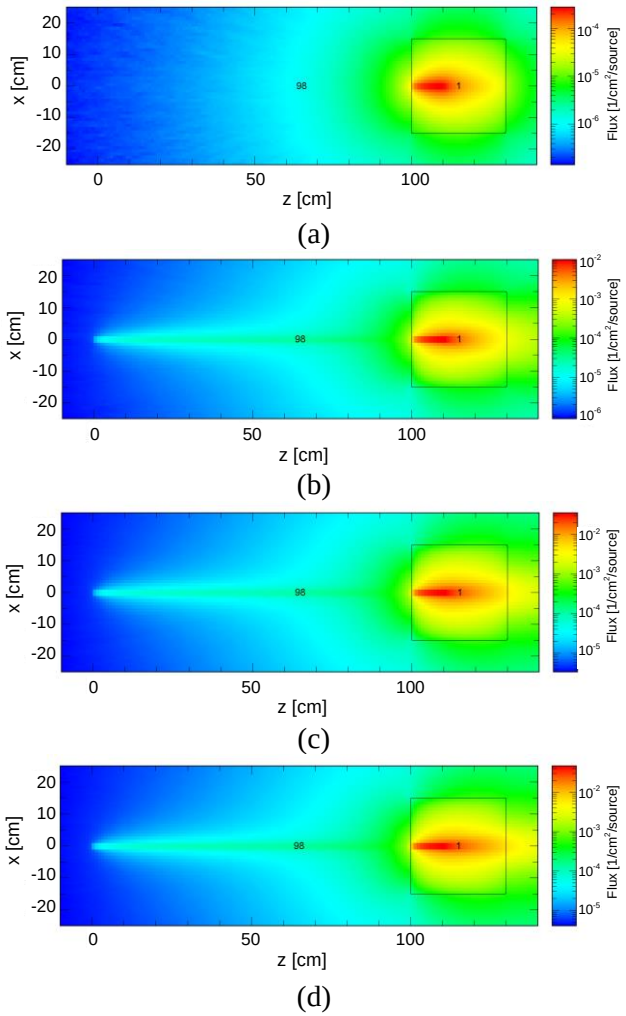

Fig. 5. Neutron fluence distributions from (a) proton (^{1}H), (b) alpha (^{4}He), (c) carbon (^{12}C), and (d) oxygen (^{16}O) at energy of 121.95 MeV/u, 122.93 MeV/u, 229.76 MeV/u and 271.59 MeV/u, respectively.

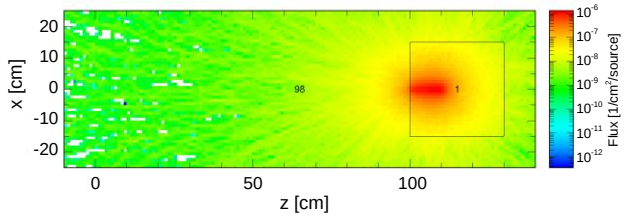

(a)

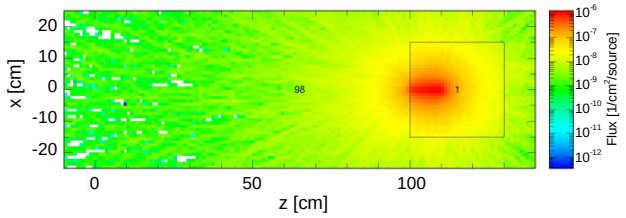

(b)

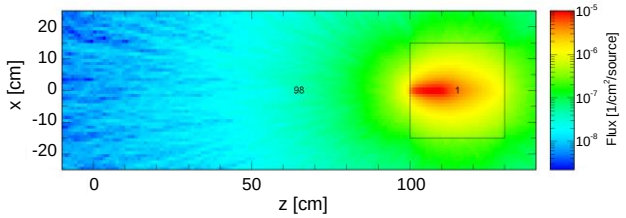

(c)

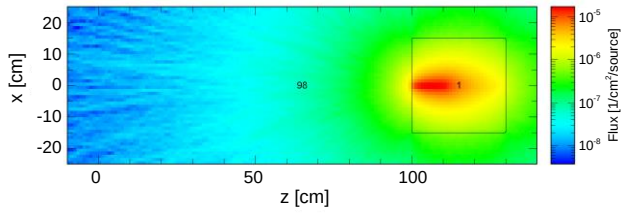

(d)

Fig. 6. Positron fluences for the energies used were (a) 121.95 MeV/u for proton (^{1}H), (b) 122.93 MeV/u for alpha (^{4}He), (c) 229.76 MeV/u for carbon (^{12}C), and (d.) 271.59 MeV/u for oxygen (^{16}O).

CONCLUSION

The Percentage Depth Dose (PDD) curves generated by PHITS reveals distinct dose deposition patterns for proton, alpha, carbon, and oxygen ions at varying energy. These curves showcase the ability of different ions to deposit energy at specific depths within the phantom, with variations observed based on energy level. The Bragg peak positions from simulations showed good agreement with experimental data (within 20%) and maintained statistical uncertainties below 0.1%, supporting the reliability of the results. Helium ions exhibited favorable clinical properties, such as reduced entrance dose and minimal scattering. The electron, positron, and neutron visualization fluence provided more insight into secondary particles produced when primary ions interact with the water phantom. Electron and positron fluence concentrations were notably higher the water phantom, with dispersion increasing with the energy of the ion source. Conversely, neutron fluence tended to concentrate along the source path until reaching the phantom, with its distribution influenced by the energy level of the ion source. Overall, these findings underscore the importance of optimizing treatment planning strategies for cancer patients.

ACKNOWLEDGMENT

The authors acknowledge the support extended by Dr. Hiroshi Takemiya, Director of the Center for Computational Science & e-Systems at the Japan Atomic Energy Agency (JAEA) for the use of JAEA Computer Programs particularly the Particle and Heavy Ion Transport code System (PHITS). We also acknowledge the DOST Learning Resource Center for the computer resources used for simulation, and the National Research Council of the Philippines for their financial support.

AUTHOR CONTRIBUTION

A. C. G. M. Dalumpines contributed to writing the original draft, software development, data curation, and investigation. B. G. F. I. Peñonal contributed to review, editing and validation. C. H. P. Aringa contributed to review, editing and investigation. D. V. C. Convicto contributed to conceptualization, review, editing, investigation and validation.

REFERENCES

1. M. C. Frese, K. Y. Victor, R. D. Stewart *et al.*, Int. J. Radiat. Oncol. Biol. Phys. **83** (2012) 442.
2. Y. Zhang, P. Trnkova, T. Toshito *et al.*, Phys. Imaging Radiat. Oncol. **26** (2023) 100439.
3. J. Xu, M. Song, Z. Fang *et al.*, J. Controlled Release **353** (2023) 699.
4. K. Parodi, A. Mairani, S. Brons *et al.*, Phys. Med. Biol. **57** (2012) 3759.
5. F. Padilla-Cabal, M. Pérez-Liva, E. Lara *et al.*, J. Radiother. Prac. **14** (2015) 311.
6. H. Zaidi and P. Andreo, Monte Carlo Calculations in Nuclear Medicine, 2nd ed, IOP Publishing, 2022.
7. D. Sheikh-Bagheri and D. W. O. Rogers, Med. Phys. **29** (2002) 391.

8. M. K. Fix, P. J. Keall, K. Dawson *et al.*, Med. Phys. **31** (2004) 3106.
9. O. E. Durán-Nava, E. Torres-García, R. Oros-Pantoja *et al*., J. Phys.: Conf. Ser. **1221** (2019) 012079.
10. B. T. Hung, T. T. Duong, and B. N. Ha, Atom Indones. **49** (2023) 13.
11. R. Sapundani, R. Ekawati, and K. M. Wibowo, Atom Indones. **47** (2021) 199.
12. F. Kurniati, F. P. Krisna, J. Junios *et al.*, Atom Indones. **47** (2021) 205.
13. T. Tessonnier, A. Mairani, S. Brons *et al*., Phys. Med. Biol. **62** (2017) 3958.
14. D. Schulz-Ertner and H. Tsujii, J. Clin. Oncol. **25** (2007) 953.
15. O. Jakel, *State of the Art in Hadron Therapy*, in: AIP Conference Proceedings, **958** (2007) 70.
16. T. Sato, K. Niita, N. Matsuda *et al*., *Overview of Particle and Heavy Ion Transport Code System PHITS*, in: Proceedings of SNA + MC 2013 - Joint International Conference on Supercomputing in Nuclear Applications and Monte Carlo (2014) 06018.
17. T. Sato, Y. Iwamoto, S. Hashimoto *et al*., J. Nucl. Sci. and Technol. **55** (2018) 684.
18. M. Puchalska and L. Sihver, Phys. Med. Biol. **60** (2015) N261.
19. D. R. Pamisa, V. Convicto, A. Lintasan *et al*., J. Phys.: Conf. Ser. **1505**, (2020) 012010.
20. V. Convicto, D. R. Pamisa, A. Lintasan *et al*., J. Phys.: Conf. Ser. **1505** (2020) 012009.